www.czasopisma.pan.pl PAN www.journals.pan.pl

ARCHIVES of FOUNDRY ENGINEERING

DE GRUYTER OPEN

ISSN (2299-2944)
Volume 17
Issue 4/2017

DOI: 10.1515/afe-2017-0122

Published quarterly as the organ of the Foundry Commission of the Polish Academy of Sciences

7 – 12

Tribological Characterization of Al-bronzes Used as Mold Materials

Ş. H. Atapek [a,] *, G. Aktaş Çelik [a], Ş. Polat [a], B. Pisarek [b,] **

[a] Department of Metallurgical and Materials Engineering, Kocaeli University, Umuttepe Campus 41380 Kocaeli, Turkey

[b] Department of Materials Engineering and Production Systems, Lodz University of Technology, Stefanowskiego Street 1/15, 90-924 Lodz-Poland

*Corresponding author. E-mail address: hatapek@gmail.com

**Honorary author. E-mail address: boguslaw.pisarek@p.lodz.pl

Received 09.05.2017; accepted in revised form 08.08.2017

Abstract

Among the copper based alloys, *Cu-Al-X* bronzes are commonly used as mold materials due to their superior physical and chemical properties. Mold materials suffer from both wear and corrosion, thus, it is necessary to know which one of the competitive phenomenon is dominant during the service conditions. In this study, tribo-corrosion behavior of CuAl10Ni5Fe4 and CuAl14Fe4Mn2Co alloys were studied and electrochemical measurements were carried out using three electrode system in 3.5 % NaCl solution in order to evaluate their corrosion resistance. In tribo-corrosion tests, alloys were tested against zirconia ball in 3.5 % NaCl solution, under 10N load with 0.04 m/s sliding speed during 300 and 600 m. The results indicate that (i) CuAl10Ni5Fe4 alloy is more resistant to NaCl solution compared to CuAl14Fe4Mn2Co alloy that has major galvanic cells within its matrix, (ii) although CuAl10Ni5Fe4 alloy has lower coefficient of friction value, it suffers from wear under dry sliding conditions, (iii) as the sliding distance increases, corrosion products on CuAl14Fe4Mn2Co surface increase at a higher rate compared to CuAl10Ni5Fe4 leading to a decrease in volume loss due to the lubricant effect of copper oxides.

Keywords: Wear resistant aluminium bronze, Mechanical properties, Microstructure, Tribological properties, Corrosion

1. Introduction

In Cu-Al bronzes, aluminium is a major alloying element and the alloys contain approximately 5-12 Al wt-%. The chemical composition also includes Fe, Ni, Mn, Si forming *Cu-Al-X* alloys and the amount of these elements is very effective in determining the final properties (strength, hardness, wear/corrosion resistance etc.) [1-3]. As suggested in several reports [4-7], not only alloy design but also a heat treatment cycle is required for Cu-Al-X alloys and a heat treatment route consisting of solution annealing, quenching and then tempering is commonly used. In order to improve the mechanical properties, following metallurgical constituents must be considered; (i) controlling the amount of hard particles within soft α-Cu [8], (ii) incorporating a combination of strengthening mechanisms like solid solution hardening, dispersion hardening and grain refining [9], (iii) embedding anti-frictional particles [10], (iv) eliminating three dimensional defects [11].

In mold technology, Cu-Al bronzes compete with several alloys, therefore, it is necessary to investigate their tribological characteristics under both dry and wet conditions. Several reports on Cu-Al bronzes [12-15] indicated that both processing conditions and final microstructure determined their corrosion or wear performance however findings lacked selection of proper bronze for industrial applications, where wear and corrosion phenomena competed. In this study, it is aimed to investigate the

tribological behaviour of *Cu-Al-X* alloys immersed into NaCl solution in order to understand the tribo-corrosion performance.

2. Experimental study

Two commercial cast and forged Cu-Al-X alloys, CuAl10Ni5Fe4 (C4) and CuAl14Fe4Mn2Co (C8), were provided from Sağlam Metal Co. and Table 1 shows their chemical composition. These alloys are high wear resistant alloys and their hardness values varied between 180-230 HB and 360-400 HB for C4 alloy and C8 alloy, respectively. The experimental study includes three stages; (i) microstructural characterization, (ii) electrochemical tests, (iii) tribological studies and characterization of the worn surfaces.

In the first stage of the study, microstructures of the alloys were microscopically characterized. Samples were metallographically prepared by grinding with 320, 600, and 1000 mesh size SiC abrasives, respectively, and then polishing with 3 µm diamond solution. Polished surfaces were then etched electrochemically using a solution consisting of NH_3 + C_2H_5OH (1:1) under 4V for 15 sec. Microstructural characterization was carried out using light microscope (LM, Olympus BX41M-LED) and scanning electron microscope (SEM, Jeol JSM 6060).

Table 1.
Chemical composition of the studied alloys (wt.-%).

Alloy	Al	Fe	Ni	Mn	Co	Cu
C4	10.00	4.80	5.00	1.50	---	balance
C8	13.80	4.00	---	2.20	1.00	balance

In the second stage of the study, Tafel method was used to investigate electrochemical response of the alloys immersed into NaCl solution (3.5 %). The cylindrical samples were coated with polyester and surface area of electrode was calculated as 0.785 cm^2. Prior to the electrochemical tests, electrode surfaces were polished and then rinsed with distilled water, degreased with ethanol and stove dried at 30 °C for 5 min. The tests were carried out in a 3-electrode cell using a Gamry reference 600 potentiostat/galvanostat, where studied alloys were used as working electrodes, platinum acted as counter electrode and saturated calomel electrode (SCE) was selected as reference electrode. The solution was mixed at 200 rpm with a magnetic stirrer during the experiments. Tafel method was carried out by sweeping the potential at a scan rate of 5 mV s^{-1} from –0.25 V to +0.25 V via SCE.

In the third stage of the study, tribological behaviour of the alloys was investigated using "ball-on-disk" type tribometer. Initially, the tribological pair (bronze/ceramic material) was tested under dry sliding condition in order to obtain coefficient of friction (COF) values as a function of sliding distance (150 m). The counterpart material was selected as ZrO_2 having 3 mm diameter and the tests were carried out under 10 N normal load, at a speed of 0.04 m/s. Then, the set-up was equipped with a home-made attachment to carry out the tribo-corrosion tests. In wet sliding tests, molded alloys having equal contact areas were fixed in a polymeric chamber and polished surfaces contacted with the counterpart material during 300 m and 600 m in NaCl solution under 10 N normal load, at a speed of 0.04 m/s (Figure 1). All test results were evaluated by (i) variation of friction coefficient (COF) as a function of sliding distance, (ii) determination of the wear rate, (iii) worn surface examinations using LM and 3D profilometer (Nanovea PS50).

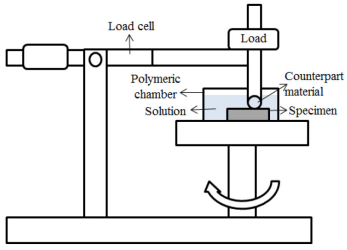

Fig. 1. A schematic illustration of a "ball-on-disc" type tribometer equipped with tribo-corrosion unit

3. Results and discussion

3.1. Microstructural characterization

The microstructure of C4 alloy is given in Figure 2a. It consists of a copper-based solid solution and various kappa phases (Ni-Al-Fe based precipitates). As reported by Al-Hashem and Riad [16], (i) kappa I phase formed directly from the melt is iron rich particle, (ii) kappa II phase has globular morphology, (iii) kappa III is a component of lamellar structure, (iv) kappa IV phase is fine iron rich particle within the matrix. C8 alloy has higher Al content compared to C4 alloy and its microstructure is given in Figure 2b. It consists of β-phase as matrix since eutectoid transformation within grains is prevented by the addition of Fe, Co, Mn and rough kappa particles (Al–Fe–Co based precipitates) [17].

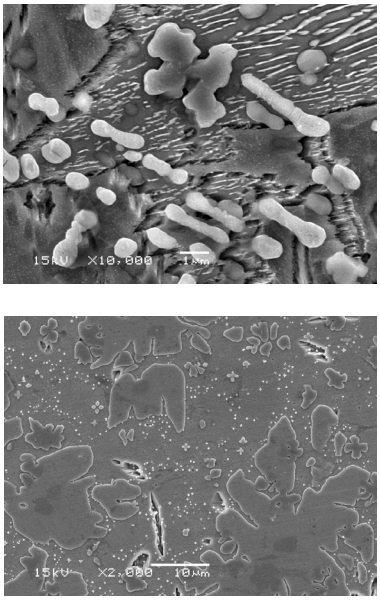

Fig. 2. SEM images showing microstructures of the studied alloys; (a) C4 and (b) C8 alloy

3.2. Evaluation of electrochemical tests

Figure 3 shows electrochemical response of the studied alloys immersed in NaCl solution and data obtained from Tafel method are listed in Table 2. According to E_{corr} (corrosion potential), I_{corr} (corrosion current density) and CR (corrosion rate) data, C4 alloy displays a superior corrosion resistance compared to C8 alloy in NaCl solution. The more anodic behaviour of C8 alloy can be explained by considering the standard electrode potentials of the elements within its matrix. In the studied alloys, copper (+0.334 V) is the most noble element having stable cathodic behaviour and aluminium is the most anodic one due to its electrode potential (-1.162 V). Among the alloying elements, nickel (-0.25 V) is another noble element to cobalt (-0.227 V), iron (-0.444) and manganese (-1.1 V) [18, 19], thus C4 alloy having 5.00 Ni wt.-% displayed more resistance to corrosion compared to C8 alloy having no nickel and higher manganese and 1.00 Co wt.-%. It is highly possible that formation of some galvanic cells (Fe-Mn, Mn-Cu and Co-Fe) causes the anodic dissolution of C8 alloy [20]. Due to the elemental partitioning several kappa phases form within C4 alloy, thus the matrix having more copper content resists to corrosion. However, C8 alloy lacks diversity of precipitates and it suffers from corrosion since the matrix consists of highly dissolved aluminium acting as anode.

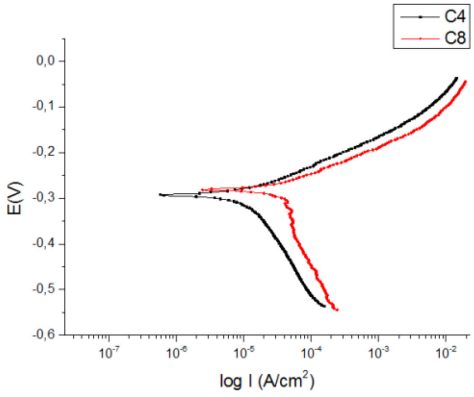

Fig. 3. Comparison of electrochemical response of studied alloys

Table 2.
Parameters obtained from Tafel method

Alloy	βc (mV)	βa (mV)	E_{corr} (mV)	I_{corr} (μA/cm²)	CR (mpy)
C4	308.40	69.00	-293	14.30	6.508
C8	175.50	90.80	-281	58.20	26.58

3.3. Tribological characterization

Initial tribological tests were carried out under dry sliding condition to determine the variation of COF values as a function of sliding distance and the diagram given in Figure 4 indicated that (i) both alloys exhibited a short run-in period and then reached to a steady-state and (ii) C4 alloy had lower COF values in steady-state regime compared to those of C8 alloy during total sliding distance. Although C8 alloy had a higher hardness value, it suffered from friction. Eutectoid structure of C4 alloy made it more resistant to wear due to its rapid work hardening characteristics under dry sliding conditions. Surface characterization of tested alloys revealed the difference in their work hardening behaviour. The wear track on worn surface of C4 alloy exhibited plastically deformed zones and the track had laminated structure (Figure 5a). However, the wear track of C8 alloy had deep grooves indicating abrasion (Figure 5b). More detailed observations done by 3D profilometrical analysis indicated that microploughing formed on the worn surface of C4 alloy and such features were the result of its higher work hardenable capacity (Figure 6a). However, 3D topography of C8 alloy had no microploughing and its surface had typical rough scratches due to abrasion (Figure 6b).

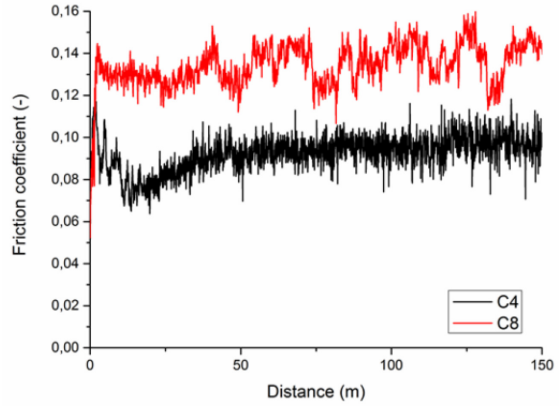

Fig. 4. Variation of COF values as a function of sliding distance for C4 and C8 alloys tested under dry sliding condition

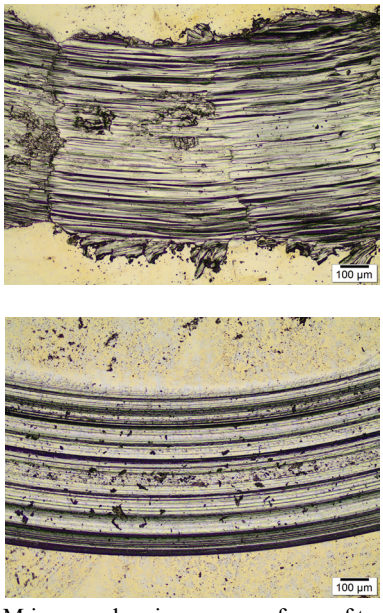

Fig. 5. LM images showing worn surfaces of tested alloys under dry sliding condition; (a) C4 and (b) C8 alloy

Following the worn surface characterization of tested alloys, wear rates were calculated according to ASTM G-99 standard and the calculations showed that C8 alloy had a lower wear rate (1.44 x 10^{-4} mm^3/Nm) compared to that of C4 alloy (2.64 x 10^{-4} mm^3/Nm). Under dry sliding conditions, although C4 alloy had lower COF value, it suffered from wear.

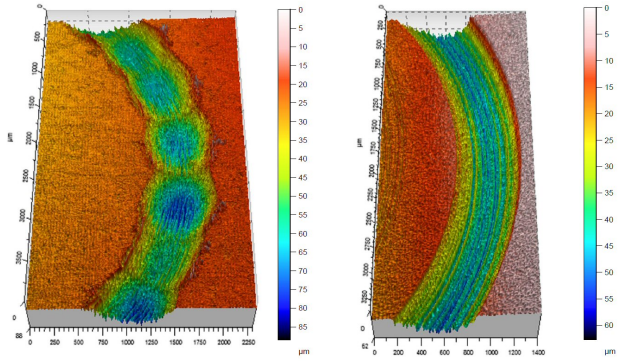

(a) (b)

Fig. 6. Comparison surface 3D topographies of tested alloys under dry sliding condition; (a) C4 and (b) C8 alloy

The alloys were also tested under wet sliding conditions. In this test, the alloy surfaces interacted with both hard ceramic counterpart and attacking Cl^- ions. COF values as a function of sliding distance were recorded for longer distances (300 and 600 m) in order to provide enough time to Cl^- attack. The total interaction time was 2 h and 4 h for tested alloys during 300 m and 600 m, respectively. The variation of COF values as a function of distance under wet sliding conditions is shown in Figure 7a and b. The diagram given in Figure 7a indicated that C8 had the shorter run-in period compared to that of C4 alloy and its max. COF value reached up to 0.13, however, max. COF value of C4 alloy was recorded as 0.10 when the sharp spikes and fluctuations were eliminated in the curve. Following the run-in period, curve of C8 alloy sharply decreased and the COF value reached to 0.06 at the initial stage of steady-state and it varied between 0.05 - 0.08. The slope of C4 curve also decreased however, there was no sharp trend after run-in period. During this run-in period, not only detachment of hard phases and agglomeration of wear debris take place but also corrosion products have possibly an effect to change 2D body to 3D body contact. This phenomenon is clearly seen in Figure 7b, especially, the curve of C4 alloy has a sharp decrease in run-in period. In shorter distance, the COF values of tested alloys in steady-state were recorded in the range of 0.05 - 0.09. In longer distance, the range of COF value for C4 alloy had no a significant change, however, COF values of C8 alloy having more corrosion potential varied in the range of 0.09 - 0.11.

LM images showing the surface features of C4 and C8 alloys tested under wet dry sliding conditions are given in Figure 8. As can be seen in the figures, the surfaces of tested alloys consist of not only a wear track but also copper based oxides visible in different colour. Due to oxidation phenomenon on the surface that interacted with corrosive media, the cupric ions can form some components like $Cu_2(OH)_3Cl$, Cu_2O and $Cu_2(OH)_3Cl$ [21, 22]. Worn surface characterization following wet sliding tests revealed that the surface contains accumulated corrosion products and as the total sliding distance increased the amount of deposits increased due to extended immersion time. The corrosion products are based on copper oxides behaving as lubricant and thus all COF values decreased under wet conditions compared to dry sliding. The deposition characteristics of the surface was also examined by 3D topographies (Figure 9) and the topographies proved that C8 alloy having more potential to be corroded had higher island-like products on the surface and the height of deposits increased as a function of total sliding distance. The volume losses under wet conditions were determined using the similar approach as in dry sliding case. At first 300 m, obtained data for volume losses were 0.0067 mm^3 and 0.0065 mm^3 for C4 and C8 alloys, respectively. These values were very close to each other and thus, did not provide information to understand the dominant factor for wear in a corrosive medium. However, tests performed for longer distances (600 m) gave a good idea to understand the dominant effect of anodic dissolution of copper based alloy in NaCl solution. In extended times, volume losses were recorded as 0.0141 mm^3 and 0.0054 mm^3 for C4 and C8 alloys, respectively. Although electrochemical tests revealed that C8 alloy suffered from corrosion, its copper based oxides covered the surface behaving as lubricant during wear test and caused the decrease of not only COF but also volume losses.

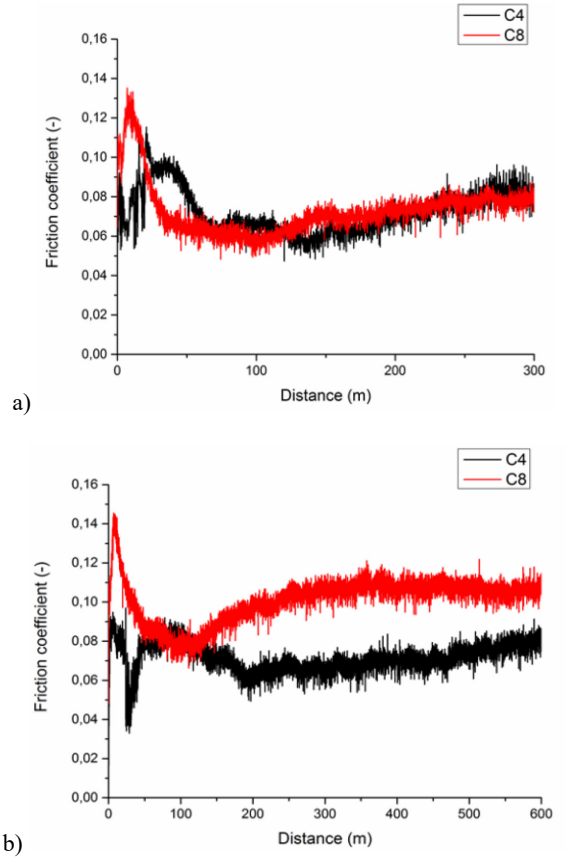

Fig. 7. Variation of COF values as a function of sliding distance for C4 and C8 alloy tested under wet sliding condition; (a) 300 m and (b) 600 m

4. Conclusions

In this study, both corrosion and wear performance of CuAl10Ni5Fe4 and CuAl14Fe4Mn2Co alloys were investigated. During investigations, initially, electrochemical tests were carried out to evaluate the anodic behaviour of alloys. Tribological tests were carried out not only in dry sliding condition but also in wet sliding condition by immersing the alloy in NaCl solution. Surface characterization was done by microscopic and 3D profilometric examination.

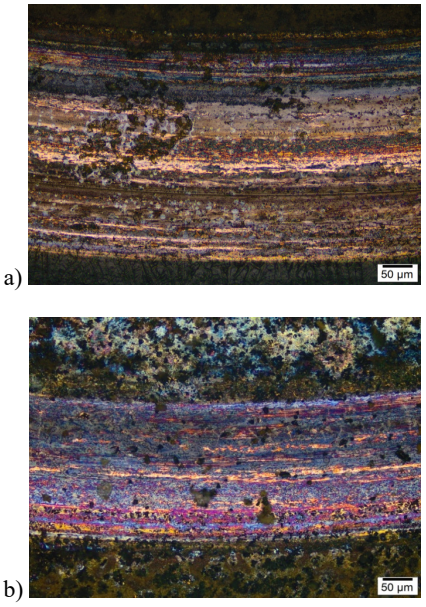

Fig. 8. LM images showing the worn surfaces of alloys immersed into NaCl solution during 600 m; (a) C4 and (b) C8 alloy

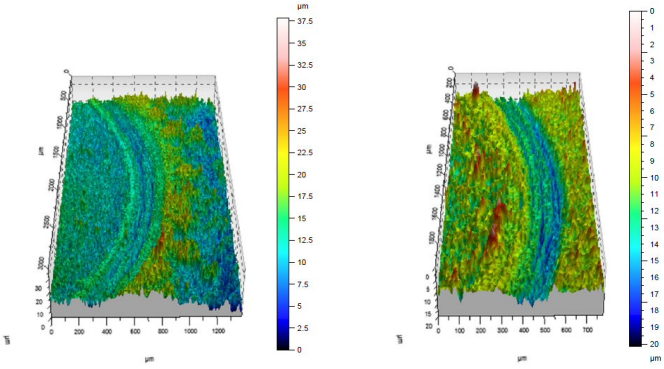

Fig. 9. Surface 3D topographies of tested alloys in NaCl solution during 600 m; (a) C4 and (b) C8 alloy

According to electrochemical test results, CuAl10Ni5Fe4 (C4) alloy is more resistant to NaCl solution compared to CuAl14Fe4Mn2Co (C8) alloy having major galvanic cells within its matrix. In dry sliding conditions, C4 alloy having more plastic deformation capability had lower COF values in total sliding distance, however, it suffered from wear due to its higher wear rate calculated according to ASTM G-99 standard. C8 alloy, with its higher hardness could be a favourable wear resistant material during interaction with rigid ceramic components. In wet sliding condition, although C8 alloy suffered from corrosion due to Cl^- ions, its copper based oxides covering the surface caused the decrease of both COF values and also volume losses.

Acknowledgements

The authors are grateful to Sağlam Metal Co. for providing the samples used in the study. The electrochemical tests were performed with the kind and professional assistance from Dr. Hatice Özkazanç. The authors are also indebted to Dr. Sinan Fidan for 3D profilometric analysis.

References

[1] Li, W.S., Wang, Z.P., Lu, Y., Gao, Y. & Xu, J.L. (2006). Preparation, mechanical properties and wear behaviors of novel aluminum bronze for dies. *Trans. Nonferrous Met. Soc. China.* 16, 607-612. DOI: 10.1016/S1003-6326(06)60107-6.

[2] Pisarek, B.P. (2013). Model of Cu-Al-Fe-Ni bronze crystallization. *Archives of Foundry Engineering*. 13(3), 72-79. DOI: 10.2478/afe-2013-0063.

[3] Labanowski, J. & Olkowski, T. (2014). Effect of microstructure on mechanical properties of BA1055 bronze castings. *Archives of Foundry Engineering.* 14(2), 73-78. DOI: 10.2478/afe-2014-0040.

[4] Wu, Z., Cheng, Y. F., Liu, L., Lv, W. & Hu, W. (2015). Effect of heat treatment on microstructure evolution and erosion-corrosion behaviour of a nickel-aluminum bronze alloy in chloride solution. *Corr. Sci*., 98, 260-270. DOI: 10.1016/j.corsci.2015.05.037.

[5] Jin, K., Qiao, Z., Zhu, S., Cheng, J., Yin, B. & Yang, J. (2016). Synthesis effects of Cr and Ag on the tribological properties of Cu-9Al-4Fe-Mn bronze under sweater condition. *Tribol. Int.*, 101, 69-80. DOI: 10.1016/j.triboint.2016.04.012.

[6] Chen, R.P., Liang, Z.Q., Zhang, W.W., Zhang, D.T., Luo, Z.Q. & Li, Y.Y. (2007). Effect of heat treatment on microstructure and properties of hot-extruded nickel-aluminium bronze. *Trans. Nonferrous Met. Soc. China*. 17, 1254-1258. DOI: 10.1016/j.corsci.2015.05.037.

[7] Li, W.S., Wang, Z.P., Lu, Y., Jin, Y.H., Yuan, L.H. & Wang, F. (2006). Mechanical and tribological properties of a novel aluminium bronze material for drawing dies. *Wear*. 261, 155-163. DOI: 10.1016/j.wear.2005.09.032.

[8] Xu, X., Lv, Y., Hu, M., Xiong, D., Zhang, L., Wang, L. & Lu, W. (2016). Influence of second phase on fatigue crack growth behaviour of nickel aluminum bronze. *Int. J. Fatigue*. 82(3), 579-587. DOI: 10.1016/j.ijfatigue.2015.09.014.

[9] Sadawy, M.M. & Ghanem, M. (2016). Grain refinement of bronze alloy by equal-channel angular pressing (ECAP) and

its effect on corrosion behaviour. *Defence Tech*. 12(4), 316-323. DOI: 10.1016/j.dt.2016.01.013.
[10] Zeng, J., Xu, J., Hua, W., Xia, L., Deng, X., Wang, S., Tao, P., Ma, X., Yao, J., Jiang, C. & Lin, L. (2009). Wear performance of the lead free tin bronze matrix composite reinforced by short carbon fibers. *Appl. Surf. Sci*. 13-14, 6647-6651. DOI: 10.1016/j.apsusc.2009.02.063.
[11] Li, Y., Ngai, T.L., & Xia, W. (1996). Mechanical, friction and wear behaviors of a novel high-strength wear-resisting aluminum bronze. *Wear*. 197, 130-136. DOI: 10.1016/0043-1648(95)06890-2.
[12] Li, W.S., Wang, Z.P., Lu, Y., Yuan, L.H., Xiao, R.Z. & Zhao, X. D. (2009). Corrosion and wear behaviors of Al-bronzes in 5.0% H_2SO_4 solution. *Trans. Nonferrous Met. Soc. China.* 19(2), 311-318. DOI: 10.1016/S1003-6326(08)60270-8.
[13] Wu, Z., Cheng, Y.F., Liu, L., Lv, W. & Hu, W. (2015). Effect of heat treatment on microstructure evolution and erosion–corrosion behavior of a nickel–aluminum bronze alloy in chloride solution. *Corr. Sci.* 98, 260-270. DOI: 10.1016/j.corsci.2015.05.037.
[14] Shi, Sun, Y., Bloyce, A. & Bell, T. (1996). Unlubricated rolling-sliding wear mechanisms of complex aluminium bronze against steel. *Wear*. 193(2), 235-241. DOI: 10.1016/0043-1648(95)06773-6.
[15] Alam, S., Masrhall, R.I. & Sasaki, S. (1996). Metallurgical and tribological investigations of aluminium bronze bushes made by a novel centrifugal casting technique. *Tribol. Int*. 29(6), 487-492. DOI: 10.1016/0301-679X(95)00108-G.
[16] Al-Hashem, A. & Riad, W. (2002). The role of microstructure of nickel-aluminum-bronze alloy on its cavitation corrosion behavior in natural seawater. *Mater. Charact*. 48, 37-41. DOI: 10.1016/S1044-5803(02)00196-1.
[17] Kudashov, D.V., Zauter, R. & Müller, H.R. (2008). Spray-formed high-aluminium bronzes. *Mater. Sci. & Eng*. A. 477, 43-49. DOI: 10.1016/j.msea.2007.06.085.
[18] Talbot, D., Talbot, J. (1998). *Corrosion Science and Technology.* USA: CRC Press.
[19] Bardal, E. (2004). *Corrosion and Protection.* London: Springer-Verlag.
[20] Ozkazanc, H. & Zor, S. (2013). Electrochemical synthesis of polypyrrole (PPy) and PPy/metal composites on copper electrode and investigation of their anticorrosive properties. *Prog. Org. Coat*. 76(4), 720-728. DOI: 10.1016/j.porgcoat.2013.01.002.
[21] Krogstad, H.N. & Johnsen, R. (2017). Corrosion properties of nickel-aluminium bronze in natural seawater – effect of galvanic coupling to UNS S31603. *Corr. Sci. in press*. DOI: 10.1016/j.corsci.2017.03.016.
[22] Wharton, J.A. & Stokes, K.R. (2008). The influence of nickel-aluminium bronze microstructure and crevice solution on the initiation of crevice condition. *Electrochim. Acta*. 53(5), 2463-2473. DOI: 10.1016/j.electacta.2007.10.047.